Mon. Not. R. Astron. Soc. **000**, 1–6 (2015) Printed 15 February 2016 (MN LATEX style file v2.2)

Using the 2-MASS Photometric Redshift Survey to optimize LIGO Follow-Up Observations

Elisa Antolini[1], Jeremy S. Heyl⋆[2]
[1] *Dipartimento di Fisica e Geologia, Università degli Studi di Perugia, I-06123 Perugia, Italia*
[2] *Department of Physics and Astronomy, University of British Columbia, 6224 Agricultural Road, Vancouver, BC V6T 1Z1, Canada*

Accepted —. Received —; in original form —

ABSTRACT
The initial discovery of LIGO on 14 September 2015 was the in-spiral merger and ring-down of the black hole binary at a distance of about 500 Mpc or a redshift of about 0.1. The search for electromagnetic counterparts for the in-spiral of binary black holes is impeded by poor initial source localizations and a lack of a compelling model for the counterpart; therefore, rapid electromagnetic follow-up is required to understand the astrophysical context of these sources. Because astrophysical sources of gravitational radiation are likely to reside in galaxies, it would make sense to search first in regions where the LIGO-Virgo probability is large and where the density of galaxies is large as well. Under the Bayesian prior assumption that the probability of a gravitational-wave event from a given region of space is proportional to the density of galaxies within the probed volume, one can calculate an improved localization of the position of the source simply by multiplying the LIGO-Virgo skymap by the density of galaxies in the range of redshifts. We propose using the 2-MASS Photometric Redshift Galaxy Catalogue for this purpose and demonstrate that using it can dramtically reduce the search region for electromagnetic counterparts.

1 INTRODUCTION

LIGO has recently begun to detect gravitational wave events from the local Universe (Abbott et al. 2016). During these initial years of gravitational astronomy, the localization of the candidate events on the sky is poor with the ninety-percent confidence regions covering hundreds or even thousands of square degrees. Finding an electromagnetic counterpart to these candidate graviational-wave events will be crucial to understanding what produces them, interpretation of the signal and to provide tests of general relativity. The ideas of how the the electromagnetic counterparts would appear are varied and uncertain. There has been substantial speculation on the electromagnetic transients associated with the mergers of binaries that include a neutron star (e.g. East et al. 2016; Kawaguchi et al. 2016; D'Orazio et al. 2016; Fernández & Metzger 2015; Mingarelli et al. 2015; Kyutoku et al. 2015; Siegel & Ciolfi 2015b,a) However,the first discovered gravitational wave event appears to be the merger of binary black holes, so the appearance and duration of the electromagnetic counterparts are especially uncertain with only a few models (e.g. Gerosa et al. 2015; Margalit & Piran 2015; Cerioli et al. 2016; Yang & Zhang 2016) Consequently, rapid electromagnetic follow-up of a large portion of the probable region would increase the chance of success in finding a counterpart. Over the large search regions and over the span of days or weeks, many electromagnetic transients typically occur, and with the wide variety of models it will be difficult to associate unambigously a particular electromagnetic event with a candidate gravitational-wave event.

The purpose of this paper is to present a strategy to alleviate both of these issues; that is, to reduce both the search region and the time required to plan and begin observations. We follow the spirit of Gehrels et al. (2015) to develop a galaxy catalogue to guide the observational plan. However, our goal here is to develop a nearly complete catalogue at the expense of having less accurate estimates of the redshifts of the galaxies within the catalogue. The accuracy of the galaxy distances needs to be only as good as the distance estmates of the gravitational-wave events. Additionally we will outline a straightforward and rapid technique to generate a nearly optimal observing plan to follow up the events rapidly (i.e. within a few seconds of the trigger).

2 BAYESIAN APPROACH TO FOLLOW-UP

Because we will be interested in the rapid follow-up of candidate gravitational-wave events, we will focussed on the rapid Bayesian reconsruction outlined by Singer & Price (2015), BAYESTAR. At the most basic level, BAYESTAR yields a probability map on the sky in the form of a HEALPpix map (Górski et al. 2005) where each pixel contains the probability $P(d|m)$ that a particular model (i.e. position on the sky) will yield the data (i.e. the observed strains on the LIGO and Virgo interferometers). To plan an observing strategy one would like the probability of a particular model (i.e.

position on the sky) given the data. We have from Bayes's theorem

$$P(\text{position}|\text{data}) = \frac{P(\text{position})P(\text{data}|\text{position})}{P(\text{data})}. \quad (1)$$

If we make the additional mild assumption that gravitational-waves originate from nearby galaxies, the probability of a given position on the sky naturally is proportional to the density (or perhaps the luminosity density) of galaxies in that direction integrated over distance range determined from the modelling of the gravitational waveform. Of course, these distance estimates will usually have large uncertainities so the distance range over which to integrate the galaxy density distribution will also be large, so highly accurate redshift information is not needed to construct $P(\text{position})$.

Furthermore, because we will ultimately be interested in which fields to observe (not which particular galaxies), accurate positions are not required in the construction of $P(\text{position})$. It is natural to sample $P(\text{position})$ also as a HEALPix grid with each pixel covering about the same solid angle as the field of view of the telescope of interest or the BAYESTAR map (a HEALPix `NSIDE` = 512 or about 50 square arcminutes per pixel), so positions no more accurate than arcminutes are required. The key to generate the observing plan rapidly is to calculate the required galaxy density maps beforehand in principle at the desired resolution (this optimization only speeds the process up slightly) for the distance ranges of interest. With the arrival of an alert, all that is required is to calculate Eq. (1) using the HEALPix maps, resample to the scale of the telescope, renormalize the probability, sort the pixels from most likely to least and output the positions to cover a given amount of cumulative probability (this entire process takes typically less than one second).

3 GALAXY CATALOGUES

To gain a picture of the local Universe, our focus will be the completness of the data rather than the accuracy of the distances and positions. Gehrels et al. (2015) combine several redshift surveys (e.g. Norberg et al. 2002; Liske et al. 2003; Driver et al. 2005; Huchra et al. 2012) that cover a large portion of the sky, but at various depths and attempt to increasing the completeness of the sample by using only the galaxies near the upper-end of the luminosity function (*i.e.* $L \sim L_*$) and ; the discovery that binary black holes with large masses (!) dominate the initial detections indicates that focussing the search on massive galaxies might not be the best strategy. After all such large black holes have not been found so far in our approximately L_*-galaxy, the Milky Way, or our neighbour, Andromeda. In fact theoretical arguments indicate that the production of such massive black holes results from the evolution of massive stars in low metallicity galaxies (Abbott et al. 2016; Eldridge & Stanway 2016) which are typically small in the local Universe (e.g. Heyl et al. 1997). Our goal is to have a nearly complete survey that attempts to be unbiased with respect to the mass of the galaxy.

We follow in spirit the work of Jarrett (2004) who used The Two Micron All Sky Survey extended source catalogue (2MASS XSC, Jarrett et al. 2000b; Skrutskie et al. 2006), and the assuption that all galaxies have the 'same K_s-band luminosity of around L_* to estimate distances to each galaxy and create sky maps of the local Universe. A substantial fraction of 2MASS has measured redshifts (e.g Huchra et al. 2012). Bilicki et al. (2014) combined the photometric data from 2MASS XSC with additional photometry the mid-infrared from WISE (Wright et al. 2010) and the optical from SuperCOSMOS (Hambly et al. 2001a,b,c). Using this multiband photometry, they trained neural networks using measured spectroscopic redshifts from SDSS (Ahn et al. 2012, 2014), 2dF (Colless et al. 2001, 2003), 6dF (Jones et al. 2004, 2009) and other catalogues to determine photometric redshifts. They also extend the photometric redshift catalogue beyond the 2MASS XSC building a three-dimensional map of the sky out to a redshift of nearly 0.2 well into the realm of the first gravitational wave event. The 2MASS Photometric Redshift (2MPZ) catalogue contains over one million galaxies with a median redshift of 0.1 with a typical scatter between the photometric and spectroscopic redshifts (where both are known) of $\sigma_z = 0.015$.

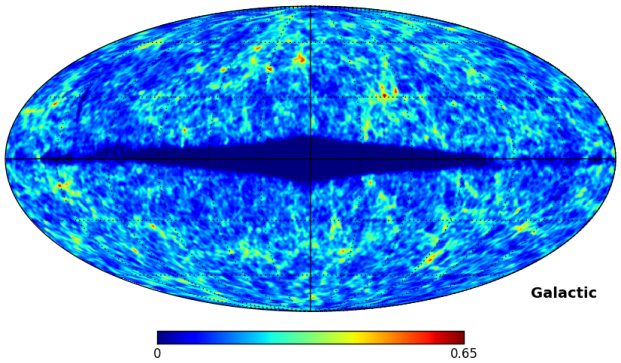

Figure 1. The relative surface density of galaxies in the 2-MASS Photometric Redshift Survey with photometric redshifts between 0.01 and 0.1, smoothed with a Gaussian of 0.6 degrees (0.01 radian).

Except for the most local sources, the estimate distances from the gravitational wave data itself have comparable errors to this, so this catalogue is sufficiently accurate to calculate the surface density of galaxies with the expected redshift range of a particular gravitational-wave detection. Furthermore, for the nearest sources, there are nearly uniform all-sky redshift surveys which would be more appropriate for this task (e.g Saunders et al. 2000; Huchra et al. 2012). Of course, all of the techniques outlined here can be applied to these more nearby catalogues to produce sky maps of even more nearby galaxies. Here we will focus on galaxies with photometric redshifts between 0.01 and 0.1 from the 2MPZ catalogue as depicted in Fig. 1. For closer galaxies the redshift error is significant, and the outer end of the range is both the median redshift of the catalogue and the typical distances of the binary-black-hole sources.

To produce this map we divided the sky into 3,145,728 regions (each of about 45 square arcminutes, four ACS fields) using a HEALPix (Górski et al. 2005) tesselation with `NSIDE` = 512. Each cell of the map simply contains the number of galaxies in the 2MPZ catalogue within the range

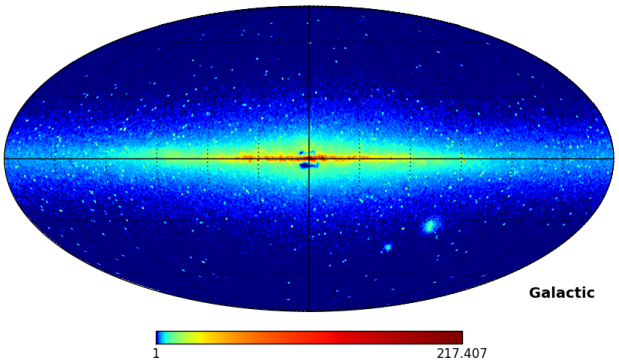

Figure 2. The relative surface brightness of stars in the 2-MASS Photometric Catalogue (Skrutskie et al. 2006) smoothed with a Gaussian of 0.03 degrees (0.005 radian).

of photometric redshift that lie within that portion of sky. We have subsequently smoothed the map with a Gaussian with $\sigma = 0.01$ radian. Typically no HEALPix pixel contains more than one galaxy from the catalogue. After smoothing we notice the large-scale structure even when we have averaged over distance. This demonstrates the potential optimization in the observing strategy by observing fields with nearby galaxies. Depending on whether one believes that the sources are associated with the visible portion of galaxies or may travel some distance from the galaxy itself before the gravitational-wave event, one would use either the raw galaxy counts or the smoothed map.

Furthermore, our choice of weighting the fields simply by the number of galaxies within each field is perhaps the most simple one. Given the type of event, one could use a map that gives small, low-metallicity galaxies more weight or weigh the galaxies by their mass or luminosity. Of course, all of these possibilities would be informed by one's prior knownledge of the source inspired by theoretical models and the hints from the waveform itself and give a better estimate of P(position). The key is to calculate these maps beforehand.

There is a further structure apparent in the map, and this is of course the zone of avoidance imposed by the disk and bulge of our Galaxy. Depending on the nature of the follow-up (*e.g.* gamma-ray and radio) observations it may make sense to include regions along the Galactic plane where one thinks nearby galaxies should be. One can attempt to probe the zone of avoidance (e.g Jarrett et al. 2000a) and future 21-cm surveys like CHIME (Vanderlinde & Chime Collaboration 2014) will also probe the large-scale structure beyond the Galactic plane. However, the existing galaxy density map as depicted in Fig. 1 can yield an estimate of the structure obscured by the Galaxy. The technique that we will use in similar to that used by Abrial et al. (2008) to inpaint the CMB anisotropies across the Galactic plane.

Here we will determine the region masked by the Galaxy by finding the region in which the density of galaxies is either less than one tenth of the mean (from Fig. 1) or in which the density of stars (from Fig. 2) is greater than a threshold that accounts for the masking of the background galaxies due to the Large Magellanic Cloud, a feature that is apparent in both figures. Both of these masks are nearly the same, so we combine them as depicted in the upper panel of Fig. 3. This region is much narrower than the infilled region of the CMB in Abrial et al. (2008), and furthermore the observed structures the galaxy map are typically longer than the width of the mask, so we can reliably estimate the hidden structures. In spite of these differences the basic strategy is similar. We assume that the underlying galaxy map (behind the Galaxy) is isotropic; therefore, it is natural to represent it as a sum of spherical harmonics; furthermore, we can argue that a small fraction of the components contain most of the power, *i.e.* the representation of the underlying map is sparse, so we can use the adaptive thresholding strategy of Bobin et al. (2007) to estimate the underlying galaxy distribution.

The technique is straightforward to describe and to implement, and we will outline it below. Let the map be given by $a(\Omega)$ and the mask by $m(\Omega)$ where $m(\Omega) = 1$ where the underlying galaxies are visible.

(i) Set an initial guess for the underlying map.

$$y_1(\Omega) = \frac{\langle m(\Omega)a(\Omega)\rangle}{\langle m(\Omega)\rangle} \tag{2}$$

(ii) Calculate the residual of the current guess

$$r_t(\Omega) = m(\Omega)a(\Omega) - y_t(\Omega) \tag{3}$$

(iii) Expand the sum of the residuals in the unmasked region and the current guess in spherical harnomics.

$$A_{lm,t} = \int d\Omega Y^*_{lm}\left[m(\Omega)r_t(\Omega) + y_t(\Omega)\right] \tag{4}$$

(iv) Keep only the components with the largest amplitudes and set the amplitudes smaller than the threshold (λ_t) to zero.

(v) Calculate the new guess from the largest components

$$y_{t+1}(\Omega) = \sum_{|A_{lm,t}|>\lambda_t} A_{lm,t}Y_{lm}(\Omega). \tag{5}$$

(vi) Decrease the threshold λ_t and repeat from step (ii) until the stopping criterion is reached.

There is of course some art in choosing the size of the underlying basis, the thresholds and the stopping criterion. Here we expand the galaxy map to $l_{\rm max} = m_{\rm max} = 64$, so there are a total of 2,145 components. The threshold is set to keep a given fraction of the components at each step. The fraction increases from $10^{-3.5}$ to $10^{-0.5}$ over 200 iterations, so the initial representations use just a few components and the number of components increases to about 680 at the final iteration, so over two thirds of the spherical harmonic components are set to zero in the final map.

From the iterative procedure above it is apparent that the value of the guess within the masked region (where $m(\Omega) = 0$) does not contribute to the residual and does not influence the solution. However, the spherical harmonics that contribute to the data near the edge of the mask do influence the guess within the masked region. The middle panel of Fig. 3 gives the initial galaxy map with the masked region filled in. There are several structures within masked region connect with the structures on either side of the Galactic plane. Finally, we can estimate the signal-to-noise of the infilled map by calculate a series of galaxy density maps by resampling the 2MPZ to obtain new catalogues, new maps and new infilled maps. The lower panel

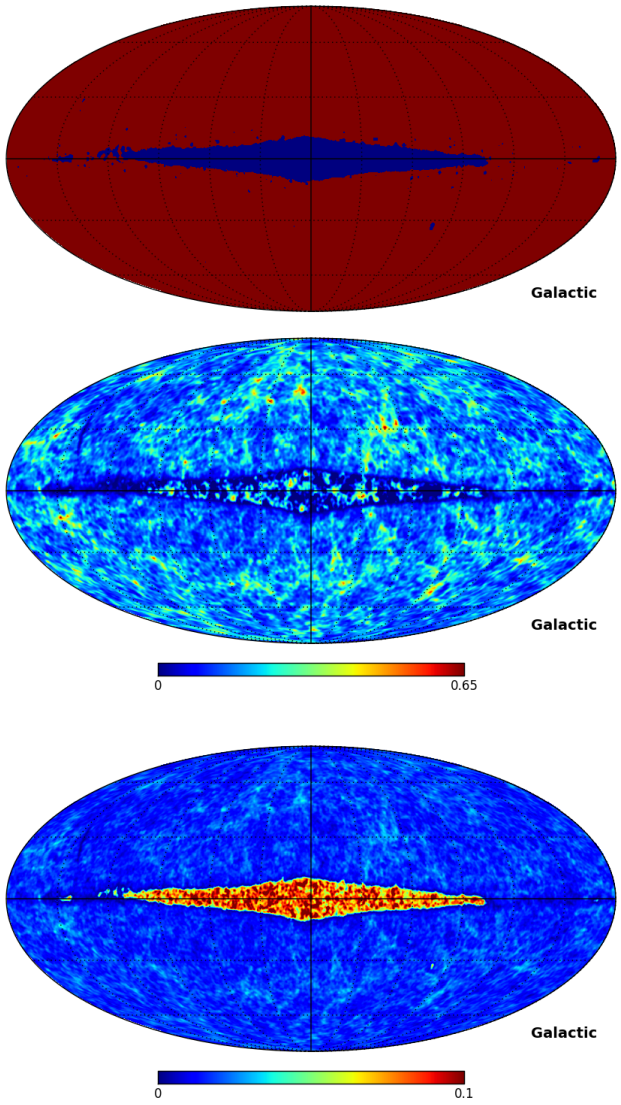

Figure 3. Upper: the mask used for the infilling procedure obtained by determining the regions where the galaxy density is less than one tenth of the mean or the star denisty lies above a given threshold (see text for details). Middle: the infilled galaxy distribution. Lower: The standard deviation of the infilled map obtained by bootstrapping the galaxy catalogue.

of Fig. 3 depicts the signal-to-noise ratio of the map. Outside of the Galactic plane the signal-to-noise almost everywhere exceeds four. In the infilled region most of the overdense structures correspond to high signal-to-noise regions and therefore may provide a reliable estimate of the regions in the zone of avoidance where $P(\text{Position})$ is large.

4 RESULTS

To assess the performance of these techinques we will focus on optical follow-up where we do not wish to observe through the zone of avoidance. We will use the Bayesian probability region calculated by the BAYESTAR algorithm (Singer & Price 2015) from Singer et al. (2014) for a LIGO-only detection, that is, before Virgo is operational. For simplicity we focus on fields of view that correspond to a particular valid value of `NSIDE` for the HEALPix map. In particular we examine a 13-square-degree field of view (`NSIDE` = 32) similar to that of LSST, 3-square-degree (`NSIDE` = 64), 0.8 and 0.2-square-degree fields of view. We quantify the performance in two ways: the time to create the optimized observing plan is typically 1-3 seconds and the decrease in the number of fields required to reach a given cumulative probability. The time to create the observing plan is typically less than the time to point the telescope and begin observations, so the strategy would be to point the telescope to the peak of the raw probability region and calculate the observing plan during the slew.

Fig. 4 depicts the results for the different sizes of fields and the possibility of using an raw (unsmoothed) and smoothed galaxy map. The upper panel gives the performance with a galaxy map restricted to the redshift range $0.03 < z < 0.04$. Here the improvement in the number of fields to observe is most dramatic. Let's start with the lowest triplet of curves that correspond to the largest field of view. Here the improvement is of using a galaxy map is modest, the number of fields to achieve a given cumulative probability decreases by about 20%. This is because most 13-square-degree regions of the sky contain a nearby galaxy. Furthermore, with such a large field of view using a smoothed galaxy map does not affect the results significantly. On the other hand, if one uses the alternative metric of what is the probabilty of that the source lies within the first field, the use of a galaxy map increases this probability from about 6.5% to 9.2%.

If we now examine the most modest field of view, the 0.2 square-degree field, we can see a more dramatic advantage of using the galaxy map. If one uses the raw galaxy map in which each observed field must contain at least one galaxy, it requires 57 fields (or about 12 square degrees) to reach half of the cumulative probability. To reach the same cumulative probability requires 186 fields (about 40 square degrees) if one uses the smoothed map and 308 fields (about 65 square degrees) without a galaxy map. For such a small field of view the effectiveness of the galaxy map is dramatic. Furthermore, the chance of the source being in the first observed field increases from 0.26% to 2.3% with the unsmoothed map. Understandably for the intermediate-sized fields of view the improvement is intermediate between that achieved for the LSST field of view and for the modest one.

If the redshift estimate for the source is somewhat less accurate perhaps $0.01 < z < 0.05$, the gains to be had by using a galaxy map are more modest as depicted in the lower panel of Fig. 4. For the 13 square-degree field of view, the improvement is especially modest; with the galaxy map eight fields are required to reach the fifty percent mark and without the map nine fields are required. For the smallest field of view, the galaxy map reduces the number of fields required to reach the fifty-percent mark from 308 to 141, a 55% reduction. With the more accurate redshift estimate the reduction was over 80%. The probability of the source lying in the first field increases from 0.26% to 0.52%. This stresses the importance of having distance estimates as early as possible in the data analysis following a burst.

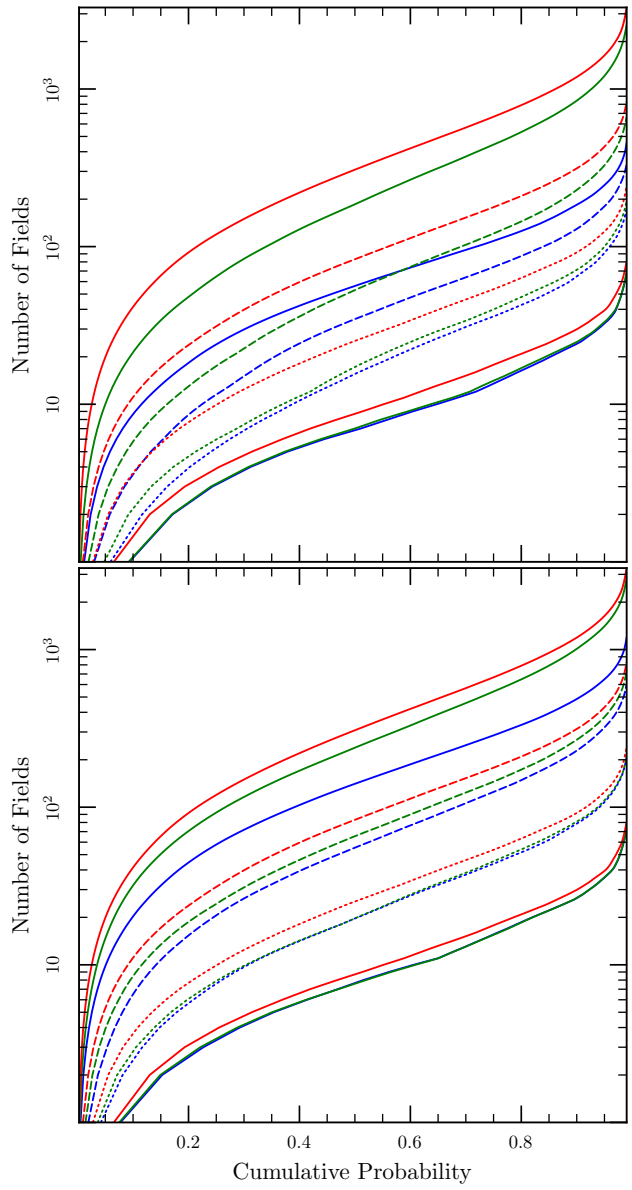

Figure 4. The number of fields required to cover the given fraction of the probablity region for a simulated LIGO detection (red curves without the galaxy map, green curves with a smoothed galaxy, blue curves with a raw galaxy map). The upper solid curves use a healpix map with about 200,000 cells, the dashed curves have about 50,000 cells, the dotted curves have about 12,000 cells and lower solid curves have about 3,000 cells, corresponding 0.2, 0.8, 3.2 and 13 square-degree fields of view. The redshift range of the galaxy map in the upper panel is $0.03 < z < 0.04$ and $0.01 < z < 0.05$ in the lowel panel.

5 CONCLUSIONS

The discovery of gravitational waves binary black hole highlights the need for rapid three-dimensional localization of gravitational-wave events to understand the astrophysical nature of these sources.

more stuff to add here

The software used in this paper is available at `http://ubc-astrophysics.github.io`. We used the VizieR Service, the NASA ADS service, the SuperCOSMOS Science Archive, the NASA/IPAC Infrared Science Archive, the HEALPy libraries and the arXiv. This work was supported by the Natural Sciences and Engineering Research Council of Canada, the Canadian Foundation for Innovation, the British Columbia Knowledge Development Fund and the Bertha and Louis Weinstein Research Fund at the University of British Columbia.

REFERENCES

Abbott, B. P., Abbott, R., Abbott, T. D., Abernathy, M. R., Acernese, F., Ackley, K., Adams, C., Adams, T., Addesso, P., Adhikari, R. X., & et al. 2016, Astrophys. J. Lett., 818, L22

Abbott, B. P. et al. 2016, Phys. Rev. Lett., 116, 061102

Abrial, P., Moudden, Y., Starck, J.-L., Fadili, J., Delabrouille, J., & Nguyen, M. K. 2008, Statistical Methodology, 5, 289

Ahn, C. P., Alexandroff, R., Allende Prieto, C., Anders, F., Anderson, S. F., Anderton, T., Andrews, B. H., Aubourg, É., Bailey, S., Bastien, F. A., & et al. 2014, Astrophys. J. Suppl., 211, 17

Ahn, C. P., Alexandroff, R., Allende Prieto, C., Anderson, S. F., Anderton, T., Andrews, B. H., Aubourg, É., Bailey, S., Balbinot, E., Barnes, R., & et al. 2012, Astrophys. J. Suppl., 203, 21

Bilicki, M., Jarrett, T. H., Peacock, J. A., Cluver, M. E., & Steward, L. 2014, Astrophys. J. Suppl., 210, 9

Bobin, J., Starck, J.-L., Fadili, J. M., Moudden, Y., & Donoho, D. L. 2007, IEEE Transactions on Image Processing, 16, 2675

Cerioli, A., Lodato, G., & Price, D. J. 2016, Mon. Not. Roy. Ast. Soc., 457, 939

Colless, M., Dalton, G., Maddox, S., Sutherland, W., Norberg, P., Cole, S., Bland-Hawthorn, J., Bridges, T., Cannon, R., Collins, C., Couch, W., Cross, N., Deeley, K., De Propris, R., Driver, S. P., Efstathiou, G., Ellis, R. S., Frenk, C. S., Glazebrook, K., Jackson, C., Lahav, O., Lewis, I., Lumsden, S., Madgwick, D., Peacock, J. A., Peterson, B. A., Price, I., Seaborne, M., & Taylor, K. 2001, Mon. Not. Roy. Ast. Soc., 328, 1039

Colless, M., Peterson, B. A., Jackson, C., Peacock, J. A., Cole, S., Norberg, P., Baldry, I. K., Baugh, C. M., Bland-Hawthorn, J., Bridges, T., Cannon, R., Collins, C., Couch, W., Cross, N., Dalton, G., De Propris, R., Driver, S. P., Efstathiou, G., Ellis, R. S., Frenk, C. S., Glazebrook, K., Lahav, O., Lewis, I., Lumsden, S., Maddox, S., Madgwick, D., Sutherland, W., & Taylor, K. 2003, ArXiv Astrophysics e-prints

D'Orazio, D. J., Levin, J., Murray, N. W., & Price, L. 2016, ArXiv e-prints

Driver, S. P., Liske, J., Cross, N. J. G., De Propris, R., & Allen, P. D. 2005, Mon. Not. Roy. Ast. Soc., 360, 81

East, W. E., Paschalidis, V., Pretorius, F., & Shapiro, S. L. 2016, Phys. Rev. D, 93, 024011

Eldridge, J. J. & Stanway, E. R. 2016, ArXiv e-prints

Fernández, R. & Metzger, B. D. 2015, ArXiv e-prints

Gehrels, N., Cannizzo, J. K., Kanner, J., Kasliwal, M. M., Nissanke, S., & Singer, L. P. 2015, ArXiv e-prints

Gerosa, D., Kesden, M., O'Shaughnessy, R., Klein, A.,

Berti, E., Sperhake, U., & Trifirò, D. 2015, Physical Review Letters, 115, 141102
Górski, K. M., Hivon, E., Banday, A. J., Wandelt, B. D., Hansen, F. K., Reinecke, M., & Bartelmann, M. 2005, Astrophys. J., 622, 759
Hambly, N. C., Davenhall, A. C., Irwin, M. J., & MacGillivray, H. T. 2001a, Mon. Not. Roy. Ast. Soc., 326, 1315
Hambly, N. C., Irwin, M. J., & MacGillivray, H. T. 2001b, Mon. Not. Roy. Ast. Soc., 326, 1295
Hambly, N. C., MacGillivray, H. T., Read, M. A., Tritton, S. B., Thomson, E. B., Kelly, B. D., Morgan, D. H., Smith, R. E., Driver, S. P., Williamson, J., Parker, Q. A., Hawkins, M. R. S., Williams, P. M., & Lawrence, A. 2001c, Mon. Not. Roy. Ast. Soc., 326, 1279
Heyl, J., Colless, M., Ellis, R. S., & Broadhurst, T. 1997, Mon. Not. Roy. Ast. Soc., 285, 613
Huchra, J. P., Macri, L. M., Masters, K. L., Jarrett, T. H., Berlind, P., Calkins, M., Crook, A. C., Cutri, R., Erdoğdu, P., Falco, E., George, T., Hutcheson, C. M., Lahav, O., Mader, J., Mink, J. D., Martimbeau, N., Schneider, S., Skrutskie, M., Tokarz, S., & Westover, M. 2012, Astrophys. J. Suppl., 199, 26
Jarrett, T. 2004, Publ. Ast. Soc. Aust., 21, 396
Jarrett, T.-H., Chester, T., Cutri, R., Schneider, S., Rosenberg, J., Huchra, J. P., & Mader, J. 2000a, Astron. J., 120, 298
Jarrett, T. H., Chester, T., Cutri, R., Schneider, S., Skrutskie, M., & Huchra, J. P. 2000b, Astron. J., 119, 2498
Jones, D. H., Read, M. A., Saunders, W., Colless, M., Jarrett, T., Parker, Q. A., Fairall, A. P., Mauch, T., Sadler, E. M., Watson, F. G., Burton, D., Campbell, L. A., Cass, P., Croom, S. M., Dawe, J., Fiegert, K., Frankcombe, L., Hartley, M., Huchra, J., James, D., Kirby, E., Lahav, O., Lucey, J., Mamon, G. A., Moore, L., Peterson, B. A., Prior, S., Proust, D., Russell, K., Safouris, V., Wakamatsu, K.-I., Westra, E., & Williams, M. 2009, Mon. Not. Roy. Ast. Soc., 399, 683
Jones, D. H., Saunders, W., Colless, M., Read, M. A., Parker, Q. A., Watson, F. G., Campbell, L. A., Burkey, D., Mauch, T., Moore, L., Hartley, M., Cass, P., James, D., Russell, K., Fiegert, K., Dawe, J., Huchra, J., Jarrett, T., Lahav, O., Lucey, J., Mamon, G. A., Proust, D., Sadler, E. M., & Wakamatsu, K.-i. 2004, Mon. Not. Roy. Ast. Soc., 355, 747
Kawaguchi, K., Kyutoku, K., Shibata, M., & Tanaka, M. 2016, ArXiv e-prints
Kyutoku, K., Ioka, K., Okawa, H., Shibata, M., & Taniguchi, K. 2015, Phys. Rev. D, 92, 044028
Liske, J., Lemon, D. J., Driver, S. P., Cross, N. J. G., & Couch, W. J. 2003, Mon. Not. Roy. Ast. Soc., 344, 307
Margalit, B. & Piran, T. 2015, Mon. Not. Roy. Ast. Soc., 452, 3419
Mingarelli, C. M. F., Levin, J., & Lazio, T. J. W. 2015, Astrophys. J. Lett., 814, L20
Norberg, P., Cole, S., Baugh, C. M., Frenk, C. S., Baldry, I., Bland-Hawthorn, J., Bridges, T., Cannon, R., Colless, M., Collins, C., Couch, W., Cross, N. J. G., Dalton, G., De Propris, R., Driver, S. P., Efstathiou, G., Ellis, R. S., Glazebrook, K., Jackson, C., Lahav, O., Lewis, I., Lumsden, S., Maddox, S., Madgwick, D., Peacock, J. A., Peterson, B. A., Sutherland, W., Taylor, K., & 2DFGRS Team. 2002, Mon. Not. Roy. Ast. Soc., 336, 907
Saunders, W., Sutherland, W. J., Maddox, S. J., Keeble, O., Oliver, S. J., Rowan-Robinson, M., McMahon, R. G., Efstathiou, G. P., Tadros, H., White, S. D. M., Frenk, C. S., Carramiñana, A., & Hawkins, M. R. S. 2000, Mon. Not. Roy. Ast. Soc., 317, 55
Siegel, D. M. & Ciolfi, R. 2015a, ArXiv e-prints
—. 2015b, ArXiv e-prints
Singer, L. P. & Price, L. R. 2015, ArXiv e-prints
Singer, L. P., Price, L. R., Farr, B., Urban, A. L., Pankow, C., Vitale, S., Veitch, J., Farr, W. M., Hanna, C., Cannon, K., Downes, T., Graff, P., Haster, C.-J., Mandel, I., Sidery, T., & Vecchio, A. 2014, Astrophys. J., 795, 105
Skrutskie, M. F., Cutri, R. M., Stiening, R., Weinberg, M. D., Schneider, S., Carpenter, J. M., Beichman, C., Capps, R., Chester, T., Elias, J., Huchra, J., Liebert, J., Lonsdale, C., Monet, D. G., Price, S., Seitzer, P., Jarrett, T., Kirkpatrick, J. D., Gizis, J. E., Howard, E., Evans, T., Fowler, J., Fullmer, L., Hurt, R., Light, R., Kopan, E. L., Marsh, K. A., McCallon, H. L., Tam, R., Van Dyk, S., & Wheelock, S. 2006, Astron. J., 131, 1163
Vanderlinde, K. & Chime Collaboration. 2014, in Exascale Radio Astronomy, Vol. 2
Wright, E. L., Eisenhardt, P. R. M., Mainzer, A. K., Ressler, M. E., Cutri, R. M., Jarrett, T., Kirkpatrick, J. D., Padgett, D., McMillan, R. S., Skrutskie, M., Stanford, S. A., Cohen, M., Walker, R. G., Mather, J. C., Leisawitz, D., Gautier, III, T. N., McLean, I., Benford, D., Lonsdale, C. J., Blain, A., Mendez, B., Irace, W. R., Duval, V., Liu, F., Royer, D., Heinrichsen, I., Howard, J., Shannon, M., Kendall, M., Walsh, A. L., Larsen, M., Cardon, J. G., Schick, S., Schwalm, M., Abid, M., Fabinsky, B., Naes, L., & Tsai, C.-W. 2010, Astron. J., 140, 1868
Yang, H. & Zhang, F. 2016, Astrophys. J., 817, 183